coatings

Article

Annealing Studies of Copper Indium Oxide ($Cu_2In_2O_5$) Thin Films Prepared by RF Magnetron Sputtering

Giji Skaria [1,*], Ashwin Kumar Saikumar [1], Akshaya D. Shivprasad [2] and Kalpathy B. Sundaram [1]

[1] Department of Electrical and Computer Engineering, University of Central Florida, Orlando, FL 32816, USA; saikumarashwin1991@knights.ucf.edu (A.K.S.); Kalpathy.Sundaram@ucf.edu (K.B.S.)
[2] School of Electrical Engineering and Computer Science, The Pennsylvania State University, University Park, PA 16802, USA; ads6067@psu.edu
* Correspondence: giji.skaria@ucf.edu

Abstract: Copper indium oxide ($Cu_2In_2O_5$) thin films were deposited by the RF magnetron sputtering technique using a Cu_2O:In_2O_3 target. The films were deposited on glass and quartz substrates at room temperature. The films were subsequently annealed at temperatures ranging from 100 to 900 °C in an O_2 atmosphere. The X-ray diffraction (XRD) analysis performed on the samples identified the presence of $Cu_2In_2O_5$ phases along with $CuInO_2$ or In_2O_3 for the films annealed above 500 °C. An increase in grain size was identified with the increase in annealing temperatures from the XRD analysis. The grain sizes were calculated to vary between 10 and 27 nm in films annealed between 500 and 900 °C. A morphological study performed using SEM further confirmed the crystallization and the grain growth with increasing annealing temperatures. All films displayed high optical transmission of more than 70% in the wavelength region of 500–800 nm. Optical studies carried out on the films indicated a small bandgap change in the range of 3.4–3.6 eV during annealing.

Keywords: $Cu_2In_2O_5$; RF sputtering; annealing studies; optical characteristics; XRD; morphology studies; optical bandgap

Citation: Skaria, G.; Saikumar, A.K.; Shivprasad, A.D.; Sundaram, K.B. Annealing Studies of Copper Indium Oxide ($Cu_2In_2O_5$) Thin Films Prepared by RF Magnetron Sputtering. *Coatings* **2021**, *11*, 1290. https://doi.org/10.3390/coatings11111290

Academic Editors: Rafal Chodun and Roman A. Surmenev

Received: 21 September 2021
Accepted: 20 October 2021
Published: 24 October 2021

1. Introduction

Transparent conducting oxides (TCOs) have a unique ability to allow visible light to pass through, and to conduct electricity. TCOs find many applications in solar cells, optical displays, reflective coatings, light emission devices, low-emissivity windows, electrochromic mirrors, UV sensors and windows, defrosting windows, electromagnetic shielding, and transparent electronics [1–6]. The bulk of research conducted on TCOs involves n-type TCOs for creating devices [7–12]. Many transparent electronic applications require the necessity of p-type TCOs. An early attempt to synthesize a p-type TCO from $CuAlO_2$ by the laser ablation method was reported by Kawazoe et al. [13]. Recently, researchers have been looking at the copper indium oxide- and copper gallium oxide-based thin film materials for possible p-type TCO applications [14–27]. Nair et al. fabricated a transparent thin-film p–n junction consisting of Ca and tin-doped $CuInO_2$ [28]. Further, Nair et al. reported the potential use of $CuInO_2$ for thermoelectric applications [29]. $Cu_2In_2O_5$ is another phase of Cu-In-based oxide. There has not been a lot of work conducted on $Cu_2In_2O_5$. Synthesis of $Cu_2In_2O_5$ has been reported only using either smeltering or chemical processes [20,21]. The chemical processes include synthesizing $Cu_2In_2O_5$ from aqueous solutions of nitrates, chlorides, and sulfates of Cu, In, and Ga [20]. At this moment, there have not been many attempts to investigate $Cu_2In_2O_5$ deposited by RF magnetron sputtering. RF magnetron sputtering allows films to be deposited with high uniformity and homogeneity as well as providing the capability to control the film thickness and deposition rate [30]. It has an additional advantage of having a low cost as well as the ability to achieve large-area deposition. In this work, the focus was on the deposition of $Cu_2In_2O_5$ by RF magnetron sputtering using a single target of Cu_2O:In_2O_3 in the ratio of 1:1. The structural and optical properties of $Cu_2In_2O_5$ thin films were investigated.

2. Experimental Details

2.1. Deposition of Copper Indium Oxide Thin Films

Copper indium oxide films were deposited by a radio frequency magnetron sputtering system using a CTI 100 cryogenic high-vacuum pump. A 600 W, 13.56 MHz RF power supply (Dressler Cesar 136 FST RF Generator, Denver, CO, USA) was used to power the MAK 2 sputter gun (San Jose, CA, USA). The Advance Energy VarioMatch-1000 matching network (Fort Collins, CO, USA) was used to match the source and the load impedance. All the depositions were performed at a power of 50 W. The power was ramped up at the rate of 1 W/s. Glass substrates were used to deposit the films for annealing studies up to 400 °C, whereas quartz substrates were used for annealing studies above 500 °C. The substrates were cleaned with acetone and methanol in an ultrasonic bath followed by rinsing using DI water. The samples were dried with nitrogen gas before loading them into the vacuum system. A 2″ powder pressed target of Cu_2O/In_2O_3 (1/1 mol%, 99.9% purity), ACI Alloy Inc. (San Jose, CA, USA), was used to deposit the films. A gap of 5 cm between the target and the substrate was maintained to achieve a uniform film thickness. A base pressure of 5×10^{-6} Torr was achieved before initiating the deposition. During the deposition, the pressure was maintained at 10 mTorr with an argon flow of 10 sccm. The deposition rate was found to be approximately 270 Å per minute. This was measured using a Veeco Dektak-150 profilometer (Plainview, NY, USA). All the depositions were conducted for 7.5 min to achieve approximately 2000 Å of film thickness. Post-deposition annealing was conducted from 100 to 900 °C for 90 min in O_2 gas flow.

2.2. Characterization of Copper Indium Oxide Thin Films

The XRD measurements were performed using a PANalytical Empyrean XRD system (Malvern Panalytical, Westborough, MA, USA), using radiation from a Cu source at 45 kV and 40 mA. The diffraction patterns were recorded between 2θ angles of 15° and 60°, and the phase information was analyzed using HighScore Plus software (Malvern Panalytical, Westborough, MA, USA). The surface morphology of the film was assessed using a field-emission scanning electron microscope, Zeiss ULTRA-55 FEG SEM (Zeiss Microscopy, White Plains, NY, USA). The optical transmission studies were performed using a Cary 100 UV–Vis spectrophotometer (Varian Analytical Instruments, Walnut Creek, CA, USA).

3. Results and Discussions

3.1. XRD Analysis

As-deposited films and films annealed up to 400 °C did not reveal any diffraction peaks indicating an amorphous nature. Although the XRD measurement was conducted between 15° and 60°, due to the presence of a broad amorphous peak related to the quartz substrates, the 2θ angle reported in Figure 1 is limited between 25° and 60°. Figure 1 shows the X-ray diffractograms of the films annealed at 500–900 °C in an O_2 atmosphere. The film annealed at 500 °C started showing low-intensity peaks related to the ($\bar{2}10$), ($\bar{5}03$), and ($\bar{3}13$) planes that have been attributed to the $Cu_2In_2O_5$ phase (JCPDSPDF# 30-0479). The films annealed at 600 °C and above showed more peaks related to $Cu_2In_2O_5$. It was observed that the peak intensity and peak sharpness increased with an increase in annealing temperature, denoting an increase in crystallinity. These identified planes match very well with the $Cu_2In_2O_5$-synthesized nanoparticles reported by Su et al. [20]. In addition to the $Cu_2In_2O_5$ phase, a peak at 30.7° (006) was identified. This can be attributed to either the In_2O_3 or $CuInO_2$ phase [31]. As-deposited films (not shown in Figure 1) did not display any diffraction peaks.

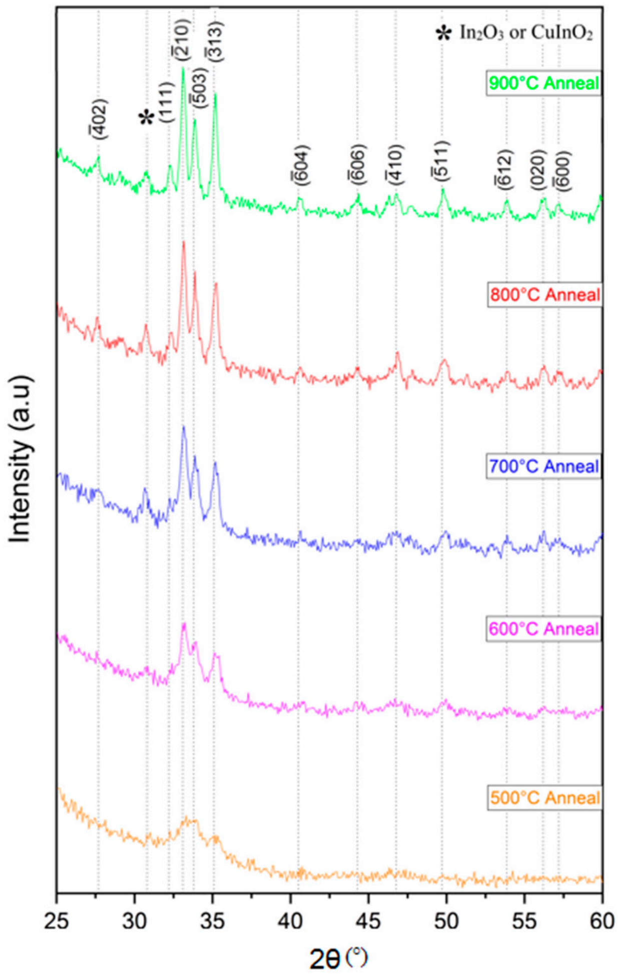

Figure 1. X-ray diffraction of the films annealed at 500–900 °C in O_2 for 90 min.

The grain sizes of the films annealed at 500–900 °C were calculated using the Debye–Scherrer equation [32].

$$D = \frac{0.9\lambda}{\beta \cos\theta} \quad (1)$$

where θ is the Bragg angle, β is the full width at half maximum of the peak, λ is the wavelength of the X-ray, and D is the average grain size. The ($\bar{3}13$) peak was used for the calculation of grain size. The average grain sizes of the $Cu_2In_2O_5$ films annealed at 500, 600, 700, 800, and 900 °C were calculated to be 10, 13, 17, 21, and 27 nm, respectively.

3.2. Morphology Studies

Figure 2 shows the SEM images of as-deposited $Cu_2In_2O_5$ thin films as well as those annealed at temperatures varying from 500 to 900 °C. Changes in the morphology were identified for the film annealed at 500–900 °C. As-deposited films and the film annealed at 500 °C displayed the presence of very small grains, as shown in Figure 2a,b. However, the films annealed at 600 °C and above showed an increase in grain size. This coincided with the results from the XRD analysis where the diffraction peaks started to appear for films annealed at 500 °C and above. Both the SEM and the XRD analysis studies indicated that a minimum of 500 °C is required to initiate nanocrystalline growth. Continuous growth in grain size was subsequently observed for the films annealed at 600–900 °C. It is worth mentioning that a pinhole-like appearance was detected in films annealed at 800 and 900 °C. Elemental analysis of all the samples was performed using EDAX incorporated in the FESEM. Nearly equal ratios of Cu:In were identified in all films.

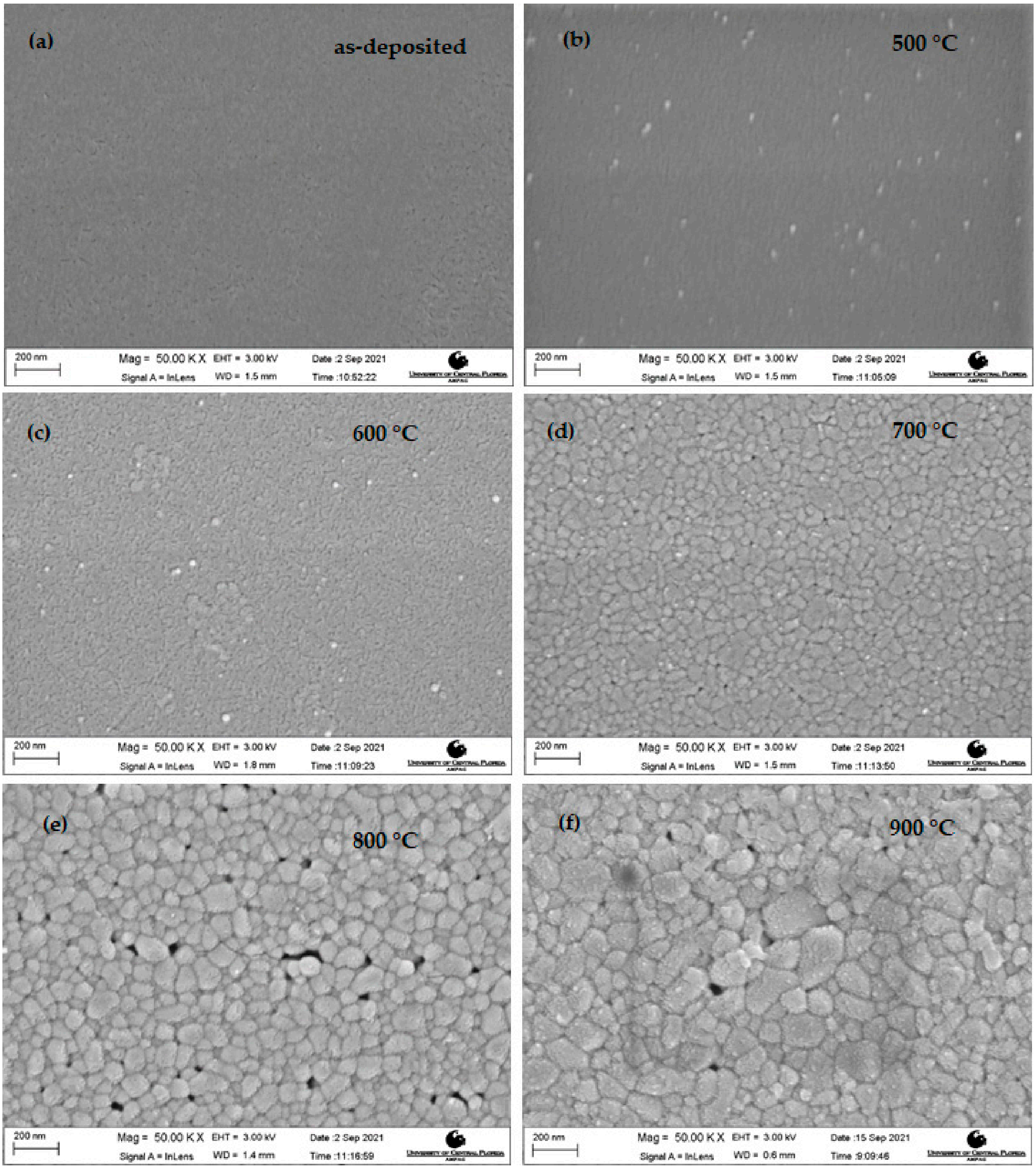

Figure 2. SEM images of $Cu_2In_2O_5$ films (**a**) as deposited and annealed at (**b**) 500 °C, (**c**) 600 °C, (**d**) 700 °C, (**e**) 800 °C, and (**f**) 900 °C.

3.3. Optical Studies

A Cary 100 UV–Vis spectrophotometer (Agilent Technologies, Santa Clara, CA, USA) was used to perform the optical characterization of the annealed $Cu_2In_2O_5$ thin films. Figure 3 shows the percent of transmission for the films deposited on glass and quartz substrates and subsequently annealed from 100 to 900 °C. Overall, the optical transmission increased for the films annealed at different temperatures. The transmission values of the annealed films were observed to vary between 70% and 90%. At a 450 nm wavelength, the films annealed at 900 °C displayed the highest transmission of 80%. However, the films annealed at 900 °C subsequently showed a decreasing trend in transmission beyond a 500 nm wavelength. This could possibly be attributed to an increase in grain size with annealing, as reported in [33,34].

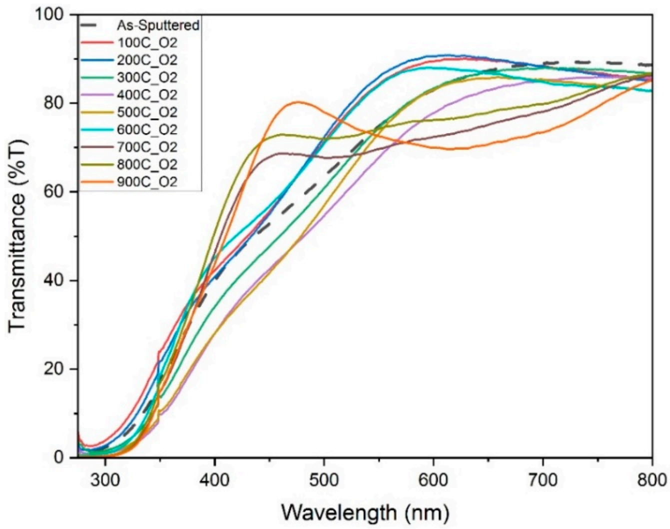

Figure 3. Optical transmission spectra of the $Cu_2In_2O_5$ thin films annealed at various temperatures.

3.4. Optical Bandgap

The optical transmission data were used to calculate the optical band gap of $Cu_2In_2O_5$ thin films using the Tauc plot method [35–37]. Since the reflectance was identified to be less than 5%, the absorption coefficient α was calculated directly from the transmission data [36]. The absorption coefficient α was calculated using Equation (2), where *d* is the thickness of the film, and *T* is the percent of transmission. The optical bandgap (Eg) was estimated from Equation (3).

$$\alpha = \frac{1}{d}\ln\left(\frac{1}{T}\right) \tag{2}$$

$$(\alpha h\nu)^{1/n} = B(h\nu - Eg) \tag{3}$$

where hν is the photon energy, B is a constant, Eg is the optical bandgap, and n = 1/2 for the direct bandgap transition. Figure 4a–j show the Tauc plot generated using the above equations. The linear region of the curve was extrapolated to the x-axis to identify the Eg value. The extrapolated values of the bandgap are listed in Table 1. The bandgap for $Cu_2In_2O_5$ thin films is reported for the first time in this work. The bandgap was in the range of 3.4–3.6 eV. It is worth mentioning that an increase in the annealing temperature did not have any major effect on the bandgap.

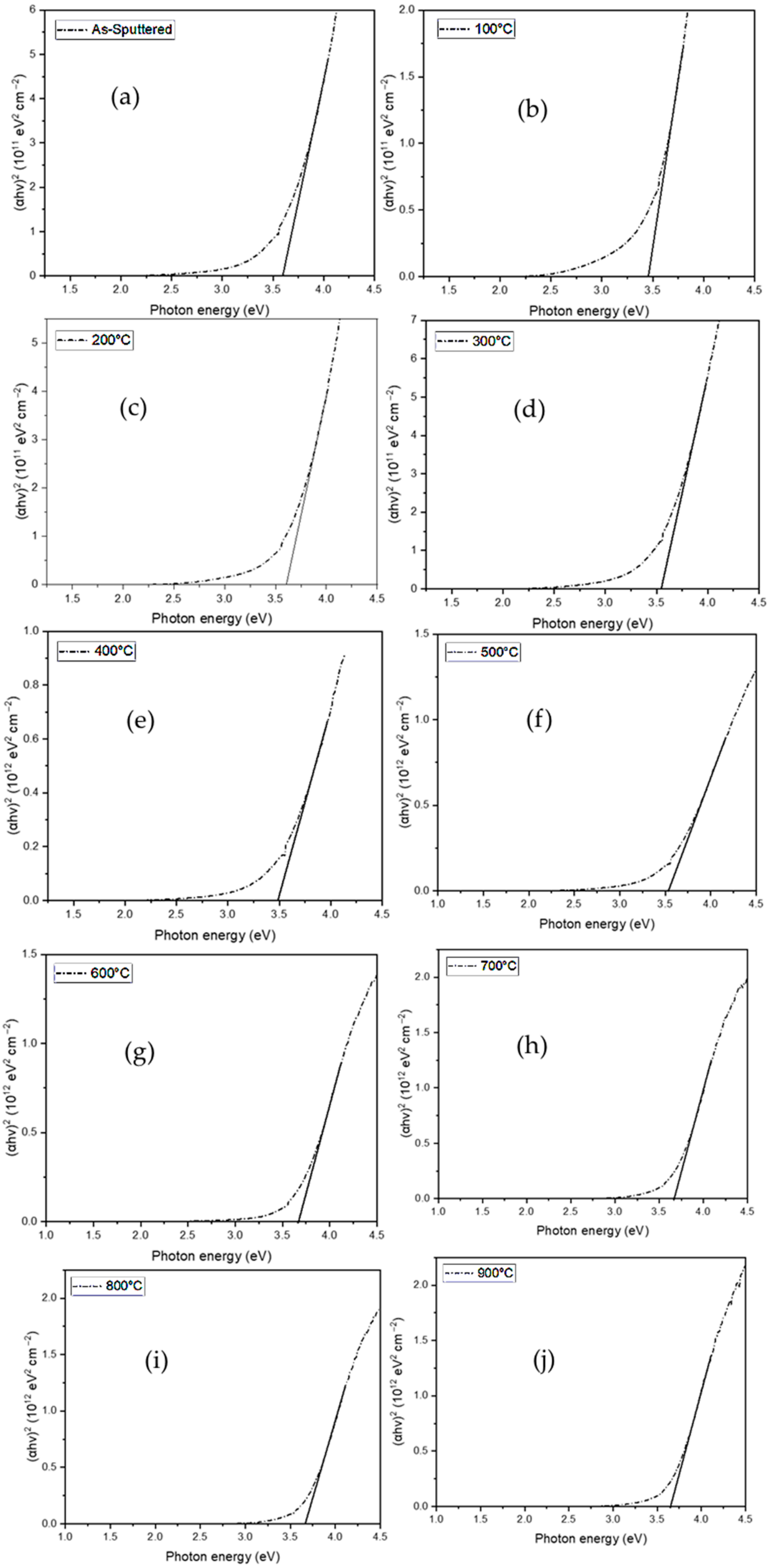

Figure 4. (**a**–**j**): Tauc plots of the $Cu_2In_2O_5$ thin films annealed at different temperatures.

Table 1. Optical bandgap values obtained for $Cu_2In_2O_5$ thin films.

Annealing Temperature (°C)	Bandgap (eV)
As deposited	3.59
100	3.45
200	3.6
300	3.54
400	3.48
500	3.53
600	3.66
700	3.66
800	3.66
900	3.64

4. Conclusions

$Cu_2In_2O_5$ thin films were deposited by the RF magnetron sputtering technique. The effects of structural, morphological, and optical properties due to post-deposition annealing at 100–900 °C with a constant O_2 flow were studied. Both the XRD analysis and the FESEM images concluded that a minimum annealing temperature of 500 °C was required to initiate the crystallization and grain growth. A further increase in the annealing temperature resulted in an increase in crystallization and grain size. The largest average grain size was observed in films annealed at 900 °C. In addition to the $Cu_2In_2O_5$ phases, the XRD results reveal the presence of an additional phase corresponding to either In_2O_3 or $CuInO_2$. Optical studies showed a bandgap of 3.4–3.6 eV for the films.

Author Contributions: Conceptualization, G.S. and K.B.S.; methodology, G.S. and A.K.S.; validation, G.S. and A.D.S.; formal analysis, G.S., A.K.S. and K.B.S.; data curation, G.S., A.K.S. and K.B.S.; writing—original draft preparation, G.S. and K.B.S.; writing—review and editing, G.S., A.K.S. and K.B.S.; visualization, G.S. and A.K.S.; supervision, K.B.S.; project administration, K.B.S. All authors have read and agreed to the published version of the manuscript.

Funding: Article processing charges were provided in part by the UCF College of Graduate Studies Open Access Publishing Fund.

Institutional Review Board Statement: Not applicable.

Informed Consent Statement: Not applicable.

Data Availability Statement: Not applicable.

Conflicts of Interest: The authors declare no conflict of interest.

References

1. Chopra, K.; Major, S.; Pandya, D. Transparent conductors—A status review. *Thin Solid Film.* **1983**, *102*, 1–46. [CrossRef]
2. Dawar, A.; Joshi, J. Semiconducting transparent thin films: Their properties and applications. *J. Mater. Sci.* **1984**, *19*, 1–23. [CrossRef]
3. Gordon, R.G. Criteria for choosing transparent conductors. *MRS Bull.* **2000**, *25*, 52–57. [CrossRef]
4. Saikumar, A.K.; Skaria, G.; Sundaram, K.B. ZnO gate based MOSFETs for sensor applications. *ECS Trans.* **2014**, *61*, 65. [CrossRef]
5. Szyszka, B.; Loebmann, P.; Georg, A.; May, C.; Elsaesser, C. Development of new transparent conductors and device applications utilizing a multidisciplinary approach. *Thin Solid Film.* **2010**, *518*, 3109–3114. [CrossRef]
6. Zhang, B.; Yu, B.; Jin, J.; Ge, B.; Yin, R. Performance of InSnZrO as transparent conductive oxides. *Phys. Status Solidi* **2010**, *207*, 955–962. [CrossRef]
7. Khan, A.; Rahman, F. Study of microstructural and optical properties of nanocrystalline indium oxide: A transparent conducting oxide (TCO). *AIP Conf. Proc.* **2019**, *2115*, 030091.
8. Nehate, S.D.; Prakash, A.; Mani, P.D.; Sundaram, K.B. Work function extraction of indium tin oxide films from MOSFET devices. *ECS J. Solid State Sci. Technol.* **2018**, *7*, P87. [CrossRef]
9. Sundaram, K.; Khan, A. Work function determination of zinc oxide films. *J. Vac. Sci. Technol. A Vac. Surf. Film.* **1997**, *15*, 428–430. [CrossRef]
10. Sundaram, K.; Khan, A.J.T.S.F. Characterization and optimization of zinc oxide films by RF magnetron sputtering. *Thin Solid Film.* **1997**, *295*, 87–91. [CrossRef]

11. Sundaresh, S.; Nehate, S.D.; Sundaram, K.B. Electrical and optical studies of reactively sputtered indium oxide thin films. *ECS J. Solid State Sci. Technol.* **2021**, *10*, 065016. [CrossRef]
12. Noh, J.H.; Ryu, S.Y.; Jo, S.J.; Kim, C.S.; Sohn, S.-W.; Rack, P.D.; Kim, D.-J.; Baik, H.K. Indium oxide thin-film transistors fabricated by RF sputtering at room temperature. *IEEE Electron. Device Lett.* **2010**, *31*, 567–569. [CrossRef]
13. Kawazoe, H.; Yasukawa, M.; Hyodo, H.; Kurita, M.; Yanagi, H.; Hosono, H.J.N. P-type electrical conduction in transparent thin films of $CuAlO_2$. *Nat. Cell Biol.* **1997**, *389*, 939–942. [CrossRef]
14. Biswas, S.K.; Sarkar, A.; Pathak, A.; Pramanik, P.J.T. Studies on the sensing behaviour of nanocrystalline $CuGa_2O_4$ towards hydrogen, liquefied petroleum gas and ammonia. *Talanta* **2010**, *81*, 1607–1612. [CrossRef]
15. Fenner, L.; Wills, A.; Bramwell, S.; Dahlberg, M.; Schiffer, P. Zero-point entropy of the spinel spin glasses $CuGa_2O_4$ and $CuAl_2O_4$. *J. Phys. Conf. Ser.* **2008**, *145*, 012029. [CrossRef]
16. Makhova, L.; Wett, D.; Lorenz, M.; Konovalov, I. X-ray spectroscopic investigation of forbidden direct transitions in $CuGaO_2$ and $CuInO_2$. *Phys. Status* **2006**, *203*, 2861–2866. [CrossRef]
17. Pilliadugula, R.; Nithya, C.; Krishnan, N.G.; Nammalwar, G. Influence of Ga_2O_3, $CuGa_2O_4$ and Cu_4O_3 phases on the sodium-ion storage behaviour of CuO and its gallium composites. *Nanoscale Adv.* **2020**, *2*, 1269–1281. [CrossRef]
18. Saikumar, A.K.; Sundaresh, S.; Nehate, S.D.; Sundaram, K.B.J.C. Properties of RF magnetron-sputtered copper gallium oxide ($CuGa_2O_4$). *Thin Film.* **2021**, *11*, 921.
19. Shi, J.; Liang, H.; Xia, X.; Li, Z.; Long, Z.; Zhang, H.; Liu, Y. Preparation of high-quality $CuGa_2O_4$ film via annealing process of Cu/β-Ga_2O_3. *J. Mater. Sci.* **2019**, *54*, 11111–11116. [CrossRef]
20. Su, C.-Y.; Chiu, C.-Y.; Chang, C.-H.; Ting, J.-M. Synthesis of $Cu_2In_2O_5$ and $CuInGaO_4$ nanoparticles. *Thin Solid Film.* **2013**, *531*, 42–48. [CrossRef]
21. Su, C.-Y.; Mishra, D.K.; Chiu, C.-Y.; Ting, J.-M. Effects of Cu_2S sintering aid on the formation of $CuInS_2$ coatings from single crystal $Cu_2In_2O_5$ nanoparticles. *Surf. Coat. Technol.* **2013**, *231*, 517–520. [CrossRef]
22. Wang, J.; Ibarra, V.; Barrera, D.; Xu, L.; Lee, Y.-J.; Hsu, J.W.P. Solution synthesized p-type copper gallium oxide nanoplates as hole transport layer for organic photovoltaic devices. *J. Phys. Chem. Lett.* **2015**, *6*, 1071–1075. [CrossRef] [PubMed]
23. Wei, H.; Chen, Z.; Wu, Z.; Cui, W.; Huang, Y.; Tang, W. Epitaxial growth and characterization of $CuGa_2O_4$ films by laser molecular beam epitaxy. *AIP Adv.* **2017**, *7*, 115216. [CrossRef]
24. Yin, H.; Shi, Y.; Dong, Y.; Chu, X. Synthesis of spinel-type $CuGa_2O_4$ nanoparticles as a sensitive non-enzymatic electrochemical sensor for hydrogen peroxide and glucose detection. *J. Electroanal. Chem.* **2021**, *885*, 115100. [CrossRef]
25. Zardkhoshoui, A.M.; Davarani, S.S. Designing a flexible all-solid-state supercapacitor based on $CuGa_2O_4$ and FeP-rGO electrodes. *J. Alloys Compd.* **2019**, *773*, 527–536. [CrossRef]
26. Zhang, K.H.L.; Xi, K.; Blamire, M.; Egdell, R.G. P-type transparent conducting oxides. *J. Phys. Condens. Mater.* **2016**, *28*, 383002. [CrossRef]
27. Singh, M.; Singh, V.N.; Mehta, B.R. Synthesis and properties of nanocrystalline copper indium oxide thin films deposited by RF magnetron sputtering. *J. Nanosci. Nanotechnol.* **2008**, *8*, 3889–3894. [CrossRef] [PubMed]
28. Nair, B.G.; Rahman, H.; Aijo, J.K.; Keerthi, K.; Shaji, G.S.O.; Sharma, V.; Philip, R.R. Calcium incorporated copper indium oxide thin films—A promising candidate for transparent electronic applications. *Thin Solid Film.* **2019**, *693*, 137673. [CrossRef]
29. Nair, B.G.; Okram, G.S.; Naduvath, J.; Shripathi, T.; Fatima, A.; Patel, T.; Jacob, R.; Keerthi, K.; Remillard, S.K.; Philip, R.R. Low temperature thermopower and electrical conductivity in highly conductive $CuInO_2$ thin films. *J. Mater. Chem. C* **2014**, *2*, 6765–6772. [CrossRef]
30. Saikumar, A.K.; Nehate, S.D.; Sundaram, K.B. Review—RF sputtered films of Ga_2O_3. *ECS J. Solid State Sci. Technol.* **2019**, *8*, Q3064–Q3078. [CrossRef]
31. Yang, B.; He, Y.; Polity, A.; Meyer, B.K. Structural, optical and electrical properties of transparent conducting $CuInO_2$ thin films prepared by RF sputtering. *MRS Proc.* **2005**, *865*, 865. [CrossRef]
32. Holzwarth, U.; Gibson, N. The Scherrer equation versus the 'Debye-Scherrer equation'. *Nat. Nanotechnol.* **2011**, *6*, 534. [CrossRef] [PubMed]
33. Ramana, C.V.; Smith, R.J.; Hussain, O.M. Grain size effects on the optical characteristics of pulsed-laser deposited vanadium oxide thin films. *Phys. Status* **2003**, *199*, R4–R6. [CrossRef]
34. Shakti, N.; Gupta, P. Structural and optical properties of sol-gel prepared ZnO thin film. *Appl. Phys. Res.* **2010**, *2*, 19. [CrossRef]
35. Duta, M.; Anastasescu, M.; Calderon-Moreno, J.M.; Predoana, L.; Preda, S.; Nicolescu, M.; Stroescu, H.; Bratan, V.; Dascalu, I.; Aperathitis, E.; et al. Sol–gel versus sputtering indium tin oxide films as transparent conducting oxide materials. *J. Mater. Sci. Mater. Electron.* **2016**, *27*, 4913–4922. [CrossRef]
36. Spence, W. The UV absorption edge of tin oxide thin films. *J. Appl. Phys.* **1967**, *38*, 3767–3770. [CrossRef]
37. Lv, J.; Huang, K.; Chen, X.; Zhu, J.; Cao, C.; Song, X.; Sun, Z. Optical constants of Na-doped ZnO thin films by sol-gel method. *Opt. Commun.* **2011**, *284*, 2905–2908. [CrossRef]